Magnetization Response of the Bulk and Supplementary Magnetic Domain Structure in High-Permeability Steel Laminations Visualized *In Situ* by Neutron Dark-Field Imaging

B. Betz,[1,4] P. Rauscher,[2] R. P. Harti,[1] R. Schäfer,[3] A. Irastorza-Landa,[4,5] H. Van Swygenhoven,[4,5] A. Kaestner,[1] J. Hovind,[1] E. Pomjakushina,[6] E. Lehmann,[1] and C. Grünzweig[1]

[1]*Paul Scherrer Institut, Laboratory for Neutron Scattering and Imaging, CH-5232 Villigen, Switzerland*
[2]*Fraunhofer IWS Dresden, Laser Ablation and Cutting, D-01277 Dresden, Germany*
[3]*Leibniz Institute for Solid State and Materials Research (IFW) Dresden, Helmholzstrasse 20, D-01069 Dresden, and University of Technology, Institute for Materials Science, D-01069 Dresden, Germany*
[4]*École polytechnique fédérale de Lausanne, NXMM laboratory, IMX, CH-1015 Lausanne, Switzerland*
[5]*Paul Scherrer Institut, Photons for Engineering and Manufacturing, CH-5232 Villigen, Switzerland*
[6]*Paul Scherrer Institut, Laboratory for Scientific Developments and Novel Materials, CH-5232 Villigen, Switzerland*

(Received 9 November 2015; revised manuscript received 3 May 2016; published 30 August 2016)

Industrial transformer cores are composed of stacked high-permeability steel laminations (HPSLs). The performance and degree of efficiency of transformers are directly determined by the magnetic properties of each HPSL. In this article, we show how the neutron dark-field image (DFI) allows for the *in situ* visualization of the locally resolved response of the bulk and supplementary magnetic domain structures in HPSLs under the influence of externally applied magnetic fields. In particular, we investigate the domain formation and growth along the initial magnetization curve up to the saturated state. For decreasing field, we visualize the recurrence of the hysteretic domain structure down to the remanent state. Additionally, the DFI allows us to derive a correlation between the grain orientation and the corresponding volume and supplementary domain structure. Furthermore, we visualize the influence of the insulation coating, introducing desired tensile stresses on the domain structures. To compare our DFI findings to traditional methods, we perform complementary surface-sensitive magneto-optical Kerr-microscopy investigations.

DOI: 10.1103/PhysRevApplied.6.024023

I. INTRODUCTION

High-permeability steel laminations (HPSLs) are produced from an iron alloy with approximately 3% of silicon. They are primarily used as core material for industrial transformer applications and remain the subject of intensive basic and applied research [1–4]. HPSLs are highly anisotropic, grain-oriented, electrical steel laminations having a sharp (110) [001] texture, the so-called Goss texture, leading to the desired magnetic properties for use in transformer cores [5–9]. A typical, 300-μm-thick, HPSL is shown in Fig. 1(a) in its coated and uncoated state. The coating, a glassy magnesium silicate layer, acts as electrical insulation to reduce eddy currents between the sheets and has a significant influence on the magnetic properties [9–13]. The lamination in its uncoated state reveals large grains with dimensions up to several centimeters as shown in Fig. 1(a). Figure 1(b) shows a sketch of the typical magnetic domain structure inside a (slightly misoriented) grain. The black and white arrows represent the magnetization direction in each domain. The misorientation angle ϑ_s is defined as the angle between the magnetic easy [001] direction of the grain and a line parallel to the surface. In this scheme, two basic magnetic domains providing a magnetization of 180° (volume domains) are shown. Small supplementary domains, consisting of surface lancets and internal, transversely magnetized domains, are superimposed to reduce the stray-field energy that is caused by the slight misorientation. The density of the supplementary domains depends on the misorientation angle [9].

Properties such as magnetic hysteresis, energy loss, and the general performance of HPSLs are usually investigated and characterized through inductive hysteresis measurements. Fluxmeters are used to measure induction. The results are well-known magnetic *B-H* loops that exhibit some *global* magnetic properties. Locally resolved information about the underlying domain structure cannot be obtained by this method. Most commonly, the surface domain structure is studied using magneto-optical Kerr microscopy [14]. The limited information depth of approximately 20 nanometers, however, allows only for an indirect interpretation of the internal volume domain structures. Furthermore, the field of view is limited to a few millimeters. Under realistic operation conditions the HPSLs are coated with an opaque layer which prohibits investigating the domain structure by conventional methods such as Kerr microscopy. It has recently been shown [15] that the coating has a direct impact of the surface and bulk domain structure. Hence, removing the coating to access

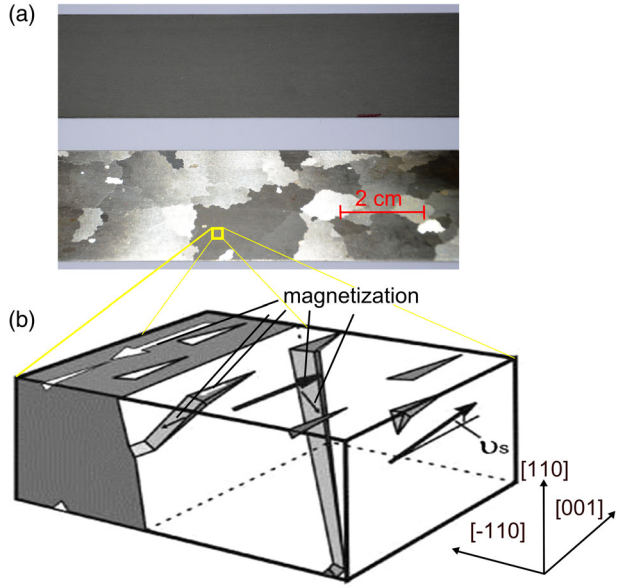

FIG. 1. (a) Optical photograph of a HPSL coated (top) and after removing the insulation coating (bottom). Large, centimeter-sized grains are visible in the uncoated state. (b) Scheme of two elongated 180° volume domains with additional supplementary domains. The supplementary domains in the volume are magnetized along the [100] and [010] "internal" easy axes. The misorientation angle ϑ_s is defined as the deviation of the magnetic easy [001] axis from the sample surface. It is conventionally defined as the angle between surface and nearest magnetic easy axis (from Ref. [9]).

the domain structure via a surface-sensitive method will not display the initial domain state of the coated steel lamination. It is also well known that the surface magnetic domain structure of a ferromagnet differs considerably from the internal domain structure due to the stray-field energy generated at a free surface. As a consequence, if one tries to visualize the internal magnetic structure by simply slicing a sample, it will reveal a newly formed surface domain structure rather than the internal domain structure. At present, 3D domain structure is mostly studied by combining the surface domain observation and domain theory. Recently, Shin *et al.* visualized the 3D microstructure of a solid Fe 6.6 at. % Si using the Libovicky method with serial sectioning [16]. Moreover, this method is destructive, as the specimen has to be cut to access the internal domains and is only applicable to materials with a certain at. % Si content.

Neutrons, on the other hand, can easily penetrate centimeter-thick metallic samples and interact (through their spin) directly with the local magnetization. With the neutron grating interferometry (NGI) technique, images of *bulk* magnetic domain structures can be obtained [17]. Bulk domain structures have been visualized in two [18–20] and even three dimensions [21]. The NGI technique has successfully been established at different neutron facilities around the world as a routine method in neutron imaging [22–25]. In this article, we present the *in situ* visualization of the formation and growth of volume and supplementary magnetic domain structures in an HPSL under the influence of externally applied magnetic fields.

II. NEUTRON GRATING INTERFEROMETER SETUP

The NGI experiments were carried out at the Swiss Spallation Neutron Source (SINQ) using the cold neutron imaging facility ICON [26]. A schematic of the measurement setup is shown in Fig. 2. The absorbing source grating G_0 (periodicity $p_0 = 1076$ μm) is placed in a monochromatic neutron beam with a wavelength of 4.1 Å ($\Delta\lambda/\lambda \approx 15\%$) provided by a velocity selector. The grating G_0 can be interpreted as an array of periodic line sources providing sufficiently high spatial coherence when illuminated with a large, centimeter-sized neutron beam. The second grating G_1 ($p_1 = 7.97$ μm), placed at a distance of $l = 5.23$ m, is used as a periodic phase modulator for the incoming neutrons. Because of the Talbot effect [27], the phase modulation is transferred into an intensity oscillation behind G_1 at a distance d_T. This intensity pattern is then analyzed by the third grating G_2 ($p_2 = 4$ μm). The NGI setup is combined with a state-of-the-art neutron imaging detection system. The images are recorded using a 100-μm-thick ^{6}LiF/ZnS scintillator screen and a digital camera [Andor NEO sCMOS, 2160×2560 pixels, pixel size 6.5 μm]. The effective spatial resolution of 70 μm is the result of intrinsic blurring of the scintillation screen, the optical system, and penumbra blurring caused by the sample to detector distance [28].

The HPSL is inserted into a magnetization frame (single sheet magnetic) which is shown in Fig. 2. The HPSLs used for the investigations is in accordance with the standard

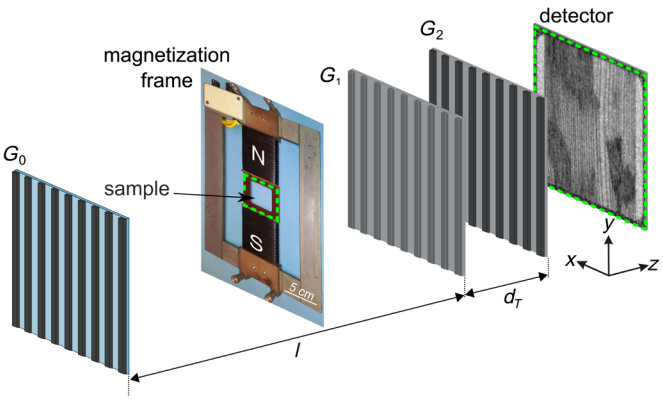

FIG. 2. Schematic of the neutron grating interferometer for the investigation of high-permeability steel laminations. The source grating G_0 is placed at a distance l from the phase grating G_1. The analyzer grating G_2 is located at the Talbot distance d_T from G_1. The magnetization frame is mounted as close as possible in front of G_1. The images are recorded by a neutron imaging detection system with a scintillator screen and a digital camera.

grade EN 10107: M 100-30 P (Thyssen-Krupp powerCore H, Grade: H 100-30, Core losses @1.7T and 50 Hz: 1.00 W/kg). The frame itself is mounted directly in front of G_1. The field of view in the experiments is 35 × 35 mm, limited by the magnetic frame window (Fig. 2, green dotted square). The coils are supplied with currents up to 4 A using a power supply [KEPCO BOP100-4ML].

III. IMPACT OF THE COATING TO THE DOMAIN STRUCTURE

Figure 3 shows the transmission images (TIs) of a coated (a) and uncoated (b) HPSL where the coating is removed chemically [29]. Independent of the presence or the absence of coating, the TIs show a very low contrast. The corresponding line profiles show an attenuation of less than 5%. In contrast to the TIs, the recorded DFIs show a pronounced contrast with dedicated features for the coated and uncoated state of the HPSL as shown in Figs. 3(c) and 3(d), respectively. The DFI contrast is a result of the scattering of neutrons at magnetic domain walls. The scattering results in a loss of coherence of the exiting neutron wave front and, consequently, in a degraded intensity oscillation in front of the detector plane. Further information about the origin of the contrast and the data processing can be found in Refs. [18–20].

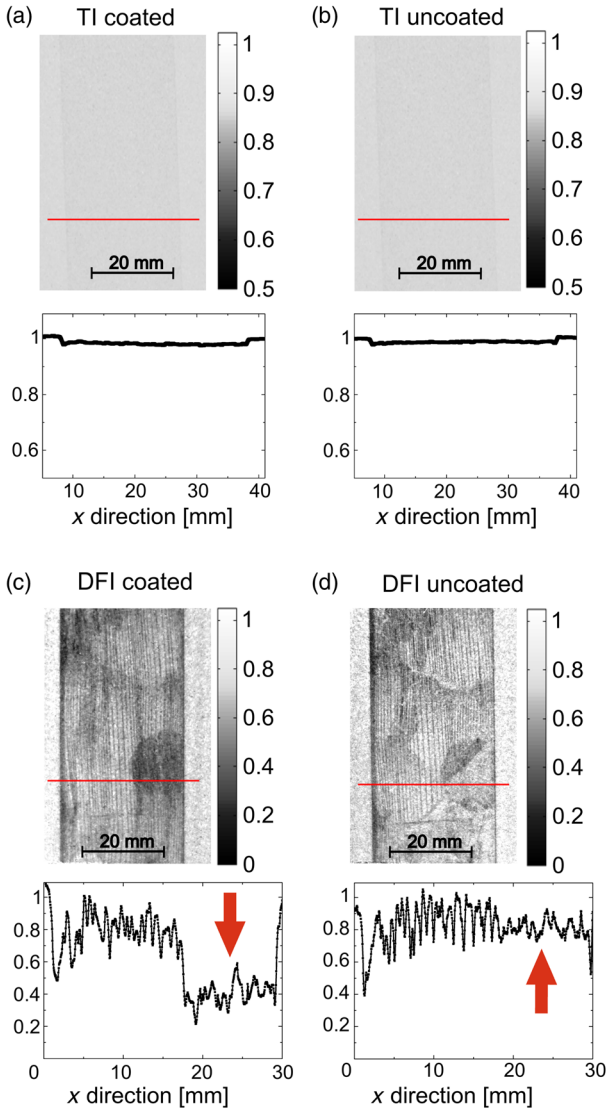

FIG. 3. TI and line profile of a coated (a) and uncoated (b) HPSL. Both TI profiles show a weak attenuation. The profiles in (c) and (d) correspond to the DFI images of the coated and uncoated state. Black line patterns represent the walls of elongated magnetic domains. Areas with reduced DFI signal (red arrow), originating from unresolved supplementary domain structures, are also visible in the corresponding line profiles.

Black vertical line patterns in the DFIs in Fig. 3(c) and 3(d) depict elongated magnetic domains, while the black lines represent the domain walls. The individual domain walls are visible because the width of these volume domains is larger than the detector resolution. Given that the magnetization of the 180° basic domains points along the crystallographic [001] direction in such material [compare Fig. 1(b)] [10], the lamination is mounted such that the [001] direction is aligned parallel to the grating line. In addition, an oval area with a decreased DFI value is observed in the lower part of the coated lamination in Fig. 3(c). This indicates a grain with a (somewhat) stronger misorientation than surrounding areas, leading to a high density of supplementary domains [compare Fig. 1(b)] that are smaller than the detector resolution. Consequently, a decreased average DFI signal is interpreted as a higher relative density of domain walls.

Comparing the HPSLs in the uncoated state [Fig. 3(d)] to the coated state, two major effects are visible. First, a qualitatively similar volume domain structure is observed in the uncoated state, but the width of the basic domains has changed. Second, the grain boundaries become more pronouncedly visible, because some volume domain walls are interrupted at the boundaries. Here, narrow supplementary domains are formed at the grain boundaries in order to reduce or avoid magnetic poles that would otherwise arise due to a flux misfit across the grain boundary. These grain-boundary domains may contain significant transversely magnetized domain volume [9]. In the DFI images, the presence of these narrow domains leads to a gray veil in (some) grain-boundary neighborhoods. In the coated state, a planar tensile stress caused by the insulation coating acts as an effective uniaxial tensile stress in the rolling direction due to the sharp Goss texture. This stress in combination with the inverse magnetostrictive effect favors the [001] direction in comparison to the transversal magnetic easy axis, and leads to a (certain) suppression of supplementary and grain-boundary domains. The removal of the coating results in an elimination of tensile stress, which explains the enhanced occurrence of the grain boundaries seen in Fig. 3(d). The reduction of supplementary domains in the coated

state leads to a refinement of the basic domain structure for the reduction of stray fields. This effect is visualized by the widening of the volume domain structure when comparing the central part next to the misoriented grain in Figs. 3(c) and 3(d).

In the oval grain in Fig. 3(c), the tensile stress of the coating seems not to be strong enough to suppress the supplementary domains due to the stronger misorientation of that grain. After removing the coating Fig. 3(d), one would even expect a darker DFI signal due to a further increased supplementary domain density. This is not observed. Furthermore, after removing the coating a diagonal line appears in that grain for an unknown reason. It is evident from Fig. 3 that different magnetic states are analyzed when investigation techniques require removing the coating to explore the underlying domain structure. A more detailed analysis where the focus is on the bulk domain-wall formation under the influence of tensile stresses is given in Ref. [15].

IV. CORRESPONDING KERR-MICROSCOPY INVESTIGATIONS

To verify the DFI findings from Fig. 3, we used Kerr microscopy to study the surface domain structure. Figure 4(a) shows the DFI of the HPSL in its uncoated state [same as in Fig. 3(d)] where the yellow box indicates the position of the following Kerr investigations. An overview Kerr image of the yellow area is shown in Fig. 4(b), and reveals large basic domains on the lower left side and an unresolvable area on the upper right side. Higher magnified images of areas 1 and 2 are shown in Figs. 4(c) and 4(d), respectively. Figure 4(c) reveals millimeter-wide basic domains. The Kerr image of the supplementary domain structure in Fig. 4(d) shows triangular-shaped lancet domains with a width, on average, of well below 50 μm. For our neutron experiments, these domains are below the detector resolution and cannot be resolved individually, leading to a reduced average DFI signal as observed in Fig. 4(a).

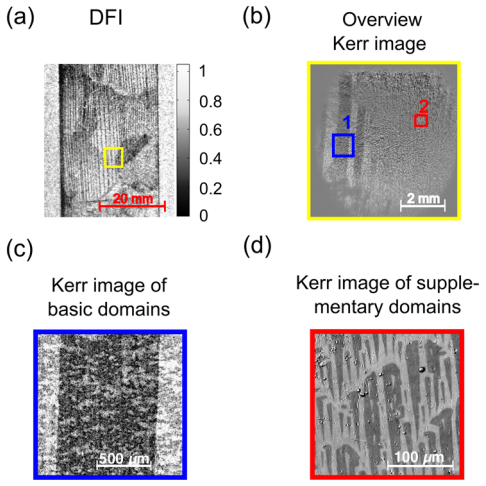

FIG. 4 (a) DFI of the HPSL showing where the Kerr images are recorded. (b) Overview Kerr image of the yellow-marked area in (a). Images (c) and (d) are magnified Kerr images of the blue (area 1) and red (area 2) areas marked in (b), respectively.

The presence of and explanation for the supplementary domains can be confirmed with crystallographic investigations using Laue x-ray diffraction (XRD). This technique provides information about the individual grain orientation. If a grain is misaligned with respect to the surface, the magnetic easy axes are misaligned, which creates energetically unfavorable magnetic stray fields. The stray-field energy is reduced by the formation of supplementary domain patterns.

However, the generation of supplementary domains also costs energy. The reduction in stray-field energy needs to exceed the energy required for the generation of supplementary domains. The stray-field energy increases with an increasing misorientation angle ϑ_s [cf. Fig. 1(b)]. As a result, supplementary domains and, consequently, a higher number of domain walls, will form in misoriented grains [9]. The threshold at which supplementary domains are built is determined by comparing the sample thickness t to a characteristic length l_0, given by

$$l_0 = \frac{\sqrt{AK}}{K_d \sin^2(\vartheta_s)}.$$

Here, A is the exchange constant, K the anisotropy constant, K_d the stray-field constant, and ϑ_s the misorientation angle. If the thickness $t > l_0$, supplementary domains will be built [10]. For the investigated HPSL having a thickness of $t = 300$ μm, the misorientation angle ϑ_s needs to exceed 1.1°. Supplementary domains are only formed for misorientation angles up to $\vartheta_s \leq 10°$ [10]. Larger misorientation angles lead to fractally branched surface domain structures.

We perform XRD Laue investigations on two positions of the HPSL, and the indexed Laue patterns can be found in the Appendix, Fig. 7. The two positions correspond to the areas 1 and 2 as shown in Fig. 4(b). Area 1 is nearly perfectly aligned. Area 2 reveals an angle of approximately $\vartheta_s \sim 8°$ between its easy axis and the surface. This misalignment explains the presence of supplementary domains which are formed to reduce stray-field energies.

V. DFI RESULTS OF MAGNETIZATION PROCESS

As stated, HPSLs are commonly characterized by recording inductive magnetic B-H loops. In Fig. 5 the first quadrant of a hysteresis loop recorded at 50 Hz is shown. Global information regarding saturation polarization, permeability, or core losses is obtained. However, the underlying domain structure inside the HPSL which

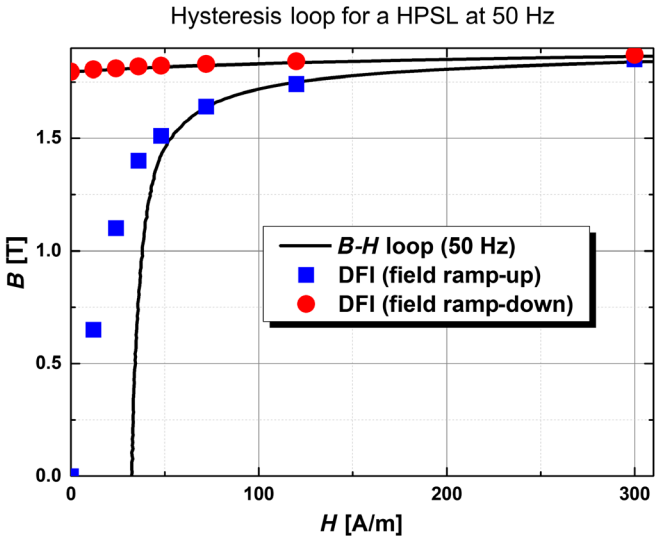

FIG. 5. Conventional B-H-loop measurements recorded at 50 Hz of a HPSL (black line). Blue squares mark where the DFIs are recorded for increasing field values. Red points mark where the DFIs for decreasing fields are obtained.

determines these global magnetic properties remains undiscovered by just recording B-H loops.

In the following section, we show how the NGI technique allows us to visualize the underlying domain formation and behavior during magnetization. For this investigation, we use a different lamination than previously (Figs. 3, 4) due to the destructive nature of the sample preparation for Kerr microscopy and the Laue technique. In contrast to Kerr-microscopy investigations, the following DFI results are recorded from an HPSL where the coating is not removed. The blue squares and red points in Fig. 5 indicate the field values where the individual DFIs are recorded.

Figure 6 shows the DFIs of the HPSL taken at different dc field values for increasing and decreasing magnetic field. The obtained DFI locally visualize the static volume domain structure in the HPSL. The left column (blue arrow) represents the DFIs of the magnetic structure during magnetization for increasing field values (blue squares in Fig. 5) along the initial magnetization curve. In the first image without applied magnetic field at $H = 0$ A/m, large elongated domain structures are visible. Again, vertical black lines represent the volume domain walls. Likewise, misoriented grains containing supplementary domains can be identified as areas with reduced DFI signal. Increasing the magnetic field to $H = 12$ A/m leads to the cancellation of several volume domain walls. The volume domain walls either end at grain boundaries or penetrate misoriented grains and build an underlying structure in addition to the supplementary domains.

Because of the magnetic flux that needs to be transported along the HPSL, domains pointing in the direction of magnetization need to grow at the cost of those pointing in

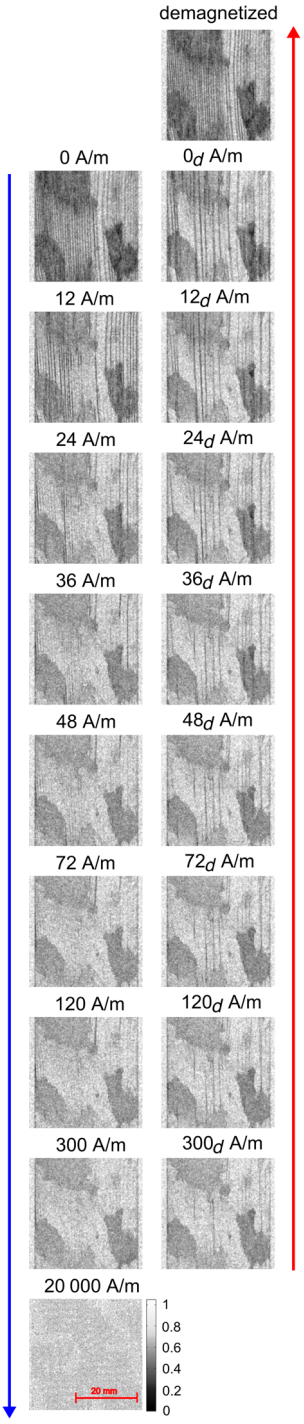

FIG. 6 *In situ* visualization of the bulk domain-wall structure of a HPSL and its changes during magnetization. In the left column, the DFIs for increasing magnetic field values from $H = 0$ A/m to $H = 20\,000$ A/m are shown consecutively. The DFIs show large vertically elongated domains, by black lines, representing the domain walls. Misoriented grains appear as dark areas in the DFIs. In the right column, the DFIs in decreasing field (denoted by index d) are shown for the same values as the DFIs in increasing fields. The remanent and demagnetized states are shown. A movie of the volume domain growth where the field is ramped from $H = 0$ A/m up to $H = 30$ A/m in steps of 1.5 A/m is in the Appendix as Video 1.

the opposite direction. The growth of domains, equivalent to the motion of the domain walls, is visible as changes in the magnetic domain structure. Because of the pinning of the volume domain walls, their sudden unsnapping (Barkhausen jumps [30]) during magnetization, and the exposure time of a single DFI (approximately 25 min), the instantaneous jumps of the domain walls appear as a continuous change of the domain structure in the corresponding DFIs. The contrast provided by the misoriented grains only changes because of the underlying volume domain structure, while the contrast originating from the supplementary domains remains. Increasing the applied magnetic field to 24, 36, and 72 A/m, consecutively, leads to a vanishing of volume domain walls starting from the center of the HPSL towards the vertical edges. No volume domain walls are present at a field of 300 A/m. Three misoriented grains are visible for fields from 72 up to 300 A/m, getting brighter with increasing field values. These three grains have different misorientations leading to different amounts of contrast reduction; hence, the DFI values directly correlate with the misorientation angle ϑ_s via the supplementary domain-wall density. This is in good agreement with recently reported, surface-sensitive Kerr imaging results on such material [31]. A fully magnetized HPSL is shown in the DFI at 20 000 A/m. Here, the HPSL is in the "single-domain" state, resulting in no visible contrast in the DFI. The fact that no contrast is generated for very high fields gives proof that the contrast in all DFIs is of magnetic origin. A movie of the volume domain growth for applied field values from $H = 0$ A/m up to $H = 30$ A/m in steps of 1.5 A/m can be found in the Appendix as Video 1.

As seen in Fig. 6, the changes of the volume domain structure take place predominantly at field values between $H = 0$ A/m and $H = 36$ A/m. The "knee" of the magnetization curve B_K is given by $B_K = (1/\sqrt{2})B_S$, where B_S is the saturation magnetization [31]. With $B_S = 1.90$ T the value of the knee results in $B_K = 1.34$ T. This corresponds to an applied field of 50 A/m. In our DFI results, the volume domain structure vanishes in the same magnetic field range.

To study the hysteretic domain-wall behavior in the HPSL, the magnetic field is decreased to the same field values as for the initial curve (red points in Fig. 5). The corresponding DFIs can be found in the right column of Fig. 6 (red arrow). The contrast of the misoriented grains with the supplementary domains reappears first at $H = 300_d$ A/m (d represents decreasing field). As seen in the B-H loop in Fig. 5, no significant flux changes occur between increasing and decreasing magnetic field values at $H = 300$ A/m, which results in a slightly different volume domain arrangement. Further decreasing the magnetic field H_d leads to a recurrence of volume domain walls. Hysteretic effects can be visualized by comparing the DFIs for the same value of the applied magnetic field for increasing and decreasing field history. The differences in the volume domain structure in the DFIs for the pairwise correlation of increasing and decreasing field values are clearly visible.

It is known [9] that the volume domain structure depends on the magnetic flux that needs to be transported over the HPSL. The magnetic flux difference ($\Delta B = B_d - B$) increases for smaller values of applied magnetic field (compare Fig. 5). This effect is similarly reflected in the individual DFIs by a smaller number of volume domains and an asymmetric, nonperiodic width distribution of volume domains in decreasing fields (especially seen in the left half). The small supplementary domains in the misaligned grains do not carry a significant magnetic flux. This results in no visible difference in contrast for the images taken with increasing or decreasing field. Only slight changes due to the underlying volume domain structure occur. These changes, in contrast, are not related to the supplementary domains themselves.

Note that the DFI at $H = 0_d$ A/m shows the remanent state of the HPSL. The initially observed magnetic state in the DFI at $H = 0$ A/m is almost entirely reproduced in the demagnetized DFI. The HPSL is demagnetized by applying an ac-magnetic field with decreasing field amplitude.

VI. SUMMARY

HPSLs are commonly used as core material of transformers and are characterized using global inductive B-H-loop measurements. The underlying physical nature of the local domain structure determines the global magnetic properties. However, the bulk magnetic domain arrangement and response cannot be analyzed through inductive investigations. Here, we use the neutron grating interferometry technique with a dark-field imaging signal to complete a detailed study of the *in situ* and locally resolved visualization of bulk magnetic domain structures and their response to externally applied magnetic fields. The behavior of the volume and supplementary domain structures could be distinguished during magnetization. Even supplementary domains, in superposition with the underlying volume domain structure, could be identified. We visualize the domain structures for the characteristic points in a hysteresis loop, including the initial magnetization, the saturation magnetization, the remanent magnetization, and the recovered demagnetized state. In contrast to the Kerr-microscopy investigations, the DFI can be recorded without removing the protective coating. Hereby, we show that the removal of the coating changes both the underlying volume and supplementary domain structures resulting from stress relief. The DFI results presented here have the potential to help engineers further develop the magnetic properties of HPSLs and help physicists better understand macromagnetic phenomena in bulk ferromagnetic materials.

APPENDIX ADDITIONAL MEASUREMENTS

1. X-ray Laue diffraction measurement

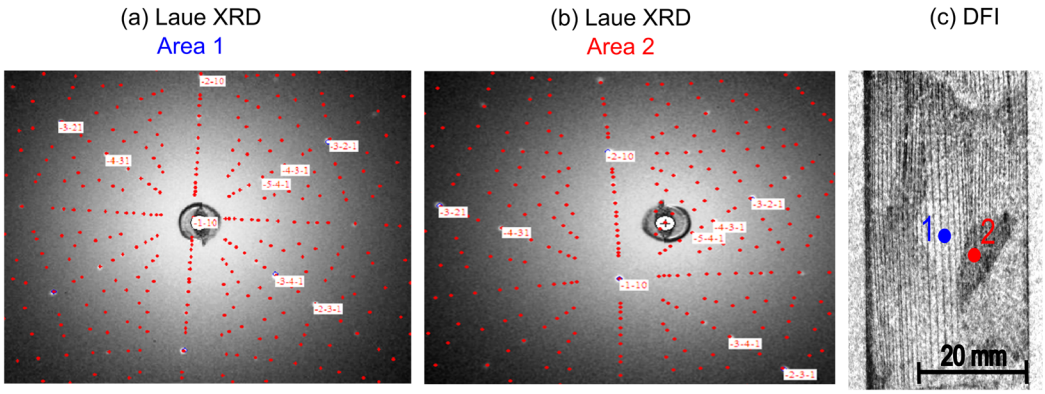

FIG. 7. (a) X-ray Laue diffraction patterns for a nearly perfect oriented grain (area 1 in Fig. 4). (b) X-ray Laue diffraction pattern for a slightly misoriented grain (area 2 in Fig. 4). The patterns are indexed using the software ORIENT-EXPRESS. From the orientation matrix of the crystal, the misorientation angle ϑ_s is calculated to 0.2° for area 1 and to 8° for area 2. This is in accordance to the experimentally observed formation of supplementary domains in the DFI. (c) Shows again the DFI of the lamination. The two areas where the XRD investigations took place are symbolized here by two colored circles.

2. Movie of the volume domain growth

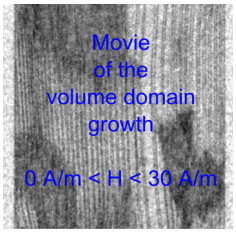

VIDEO 1. Movie of the volume domain growth in a HPSL. The field is ramped from $H = 0$ A/m up to $H = 30$ A/m in steps of 1.5 A/m.

[1] I. Gutierrez-Urrutia, A. Böttcher, L. Lahn, and D. Raabe, Microstructure–magnetic property relations in grain-oriented electrical steels: Quantitative analysis of the sharpness of the Goss orientation, J. Mater. Sci. **49**, 269 (2014).

[2] W. C. Hsu, P. L. Sun, P. W. Kao, and L. Chan, Correlation between the deformation microstructure after rolling and the recrystallization nucleation of a non-oriented electrical steel, IOP Conf. Ser.: Mater. Sci. Eng. **89**, 012027 (2015).

[3] I. Gutierrez-Urrutia, A. Böttcher, L. Lahn, and D. Raabe, Effects of pulsed magnetic annealing on Goss texture development in the primary recrystallization of grain-oriented electrical steel, J. Mater. Sci. **47**, 4110 (2012).

[4] M. Takashima, H. Inoue, and S. Okabe, Grain oriented electrical steel sheet, U.S. Patent No. 8,568,857 B2 (29 October 2013).

[5] S. Taguchi, T. Yamamoto, and A. Sakakura, New grain-oriented silicon steel with high permeability "orientcore HI-B", IEEE Trans. Magn. **10**, 123 (1974).

[6] N. P. Goss, Electrical sheet and method and apparatus for its manufacture and test, U.S. Patent No. 1,965,559 (3 July 1934).

[7] S. Mishra, C. Därmann, and K. Lücke, On the development of the Goss texture in iron-3% silicon, Acta Metall. **32**, 2185 (1984).

[8] K. I. Arai, and K. Ishiyama, Rolled texture and magnetic properties of 3% silicon steel, J. Appl. Phys. **64**, 5352 (1988).

[9] A. Hubert and R. Schaefer, *Magnetic Domains* (Springer, Berlin Heidelberg, 1998).

[10] C. Holt and J. A. Robey, The AC magnetostriction of 3.25% grain-oriented silicon-iron under combined longitudinal, and normal compressive stress, IEEE Trans. Magn. **5**, 384 (1969).

[11] E. Beyer, L. Lahn, C. Schepers, and T. Stucky, The influence of compressive stress applied by hard coatings on the power loss of grain oriented electrical steel sheet, J. Magn. Magn. Mater. **323**, 1985 (2011).

[12] W. D. Corner and J. J. Mason, The effect of stress on the domain structure of goss textured silicon-iron, Br. J. Appl. Phys. **15**, 709 (1964).

[13] A. J. Moses, Effects of applied stress on the magnetic properties of high permeability silicon-iron, IEEE Trans. Magn. **15**, 1575 (1979).

[14] R. Schäfer and S. Schinnerling, Bulk domain analysis in FeSi-crystals, J. Magn. Magn. Mater. **215**, 140 (2000).
[15] B. Betz, P. Rauscher, R. P. Harti, R. Schäfer, H. Van Swygenhoven, A. Kaestner, J. Hovind, E. Lehmann, and C. Grünzweig, *In-situ* visualization of stress-dependent bulk magnetic domain formation by neutron grating interferometry, Appl. Phys. Lett. **108**, 012405 (2016).
[16] S. Shin, R. Schaefer, and B. C. De Cooman, Three-dimensional visualization of the magnetic microstructure in bulk Fe-6.6 pct Si, Metall. Mater. Trans. A **44**, 4239 (2013).
[17] F. Pfeiffer, C. Grünzweig, O. Bunk, G. Frei, E. Lehmann, and C. David, Neutron Phase Imaging and Tomography, Phys. Rev. Lett. **96**, 215505 (2006).
[18] C. Grünzweig, C. David, O. Bunk, M. Dierolf, G. Frei, G. Kühne, R. Schäfer, S. Pofahl, H. M. R. Rønnow, and F. Pfeiffer, Bulk magnetic domain structures visualized by neutron dark-field imaging, Appl. Phys. Lett. **93**, 112504 (2008).
[19] C. Grünzweig *et al.*, Neutron Decoherence Imaging for Visualizing Bulk Magnetic Domain Structures, Phys. Rev. Lett. **101**, 025504 (2008).
[20] C. Grünzweig, C. David, O. Bunk, J. Kohlbrecher, E. Lehmann, Y. W. Lai, R. Schäfer, S. Roth, P. Lejcek, J. Kopecek, and F. Pfeiffer, Visualizing the propagation of volume magnetization in bulk ferromagnetic materials by neutron grating interferometry, J. Appl. Phys. **107**, 09D308 (2010).
[21] I. Manke *et al.*, Three-dimensional imaging of magnetic domains, Nat. Commun. **1**, 125 (2010).
[22] C. Grünzweig, F. Pfeiffer, O. Bunk, T. Donath, G. Kühne, G. Frei, M. Dierolf, and C. David, Design, fabrication, and characterization of diffraction gratings for neutron phase contrast imaging, Rev. Sci. Instrum. **79**, 053703 (2008).
[23] S. W. Lee, D. S. Hussey, D. L. Jacobson, C. M. Sim, and M. Arif, Development of the grating phase neutron interferometer at a monochromatic beam line, Nucl. Instrum. Methods Phys. Res., Sect. A **605**, 16 (2009).
[24] S. W. Lee, Y. K. Jun, and O. Y. Kwon, A neutron dark-field imaging experiment with a neutron grating, interferometer at a thermal neutron beam line at HANARO, J. Korean Phys. Soc. **58**, 730 (2011).
[25] E. Calzada, F. Gruenauer, M. Mühlbauer, B. Schillinger, and M. Schulz, New design for the ANTARES-II facility for neutron imaging at FRM II, Nucl. Instrum. Methods Phys. Res., Sect. A **605**, 50 (2009).
[26] A. KaestnerA. P. Kaestner, S. Hartmann, G. Kühne, G. Frei, C. Grünzweig, L. Josic, F. Schmid, and E. H. Lehmann, The ICON beamline—A facility for cold neutron imaging at SINQ, Nucl. Instrum. Methods Phys. Res., Sect. A **659**, 387 (2011).
[27] H. F. Talbot, Facts relating to optical science, Philos. Mag. **9**, 401 (1836).
[28] C. Gruenzweig, G. Frei, E. Lehmann, G. Kühne, and C. David, Highly absorbing gadolinium test device to characterize the performance of neutron imaging detector systems, Rev. Sci. Instrum. **78**, 053708 (2007).
[29] The coating is removed by chemical etching using hydrochloric acid diluted with water.
[30] D. Marko, I. Soldatov, M. Tekielak, and R. Schäfer, Stray-field-induced Faraday contributions in wide-field Kerr microscopy and -magnetometry, J. Magn. Magn. Mater. **396**, 9 (2015).
[31] E. Kneller, *Ferromagnetismus* (Springer, Berlin, 1962).